

Improved Photoresponse of Porous Silicon Photodetectors by Embedding CdS Nanoparticles

Ahmed N. Abd*

Physics Department, Faculty of Science, University of Al- Mustansiriyah, Baghdad, Iraq.

Received: 9 Aug. 2015, Revised: 22 Sep. 2015, Accepted: 24 Sep. 2015.

Published online: 1 Jan. 2016.

Abstract: In this research, the nanocrystalline porous silicon (PSi) films are prepared by electrochemical etching of p types silicon wafers with 15 mA/cm^2 etching current densities and 15 min etching time on the formation nanosized pore array PSi was characterized by the measurement of XRD, FTIR spectroscopy and atomic force microscopy properties (AFM). We have estimated crystallites size from X-Ray diffraction about nanoscale for PSi and Atomic Force microscopy confirms the nanometric size Chemical fictionalization during the electrochemical etching show on the surface chemical composition of PSi. The atomic force microscopy investigation shows the rough silicon surface. Also, it is reported the preparation of colloidal CdS nanoparticles NPs prepared by laser ablation in liquid (LAL) technique by irradiating with a Nd:YAG laser pulses CdS target immersed in methanol and varying the laser fluence 1.32 J/cm^2 . The structural, morphological and optical of CdS NPs has been studied. XRD measurement disclosed that the CdS NPs were of wurtzite hexagonal crystal structure. Transmission electron microscopy (TEM) investigation revealed that the synthesized CdS particles are spherical and have an average particle size in the range of (25 nm). AFM investigations showed that the produced CdS particles have ball- shape with good disposability. The energy band gap of CdS NPs prepared with 1.32 J/cm^2 laser fluence has been determined from optical properties and found to be in the range (2.9 eV). Optical constants of CdS NPs were determined from transmittance and reflectance spectra. The effect of CdS NPs diffusion on properties of PSi Photodetector have reported which reveals that improving in (Al/PSi/Si/Al). The results show that a linear relationship between C^{-2} and reverse bias voltage was obtained. The built-in potential have values depending on the etching time current density and laser fluence .Al/CdSe/PSi/Si/Al photodetector hetrojunction have two peaks of response located at 415 nm and (700 -800nm) with max sensitivity $\approx 0.6 \text{ A/W}$. The maximum specific detectivity is $6.8 \times 10^{12} \text{ cm. Hz}^{1/2} \text{ W}^{-1}$ at $\approx 770 \text{ nm}$ wavelength .

Keywords: PSi, CdS, Nanoparticles, XRD, SEM, Photodetector

1 Introduction

The use of semiconducting materials in the form of thin films now a day's occupy prominent place in the basic as well as applied research. It is a technologically useful material due to wide band gap of 2.42 eV, as many devices such as electronic devices including light emitting diodes, single electron transistors and field effect transistor [1] sensors [2] window materials [3]. CdS solar cell has several years been considered to be a promising alternative to the more widely used silicon devices [4]. The efficiency and performance of the devices depends on the optical and electrical properties of the thin films. So that attempt tried to understand the role of substrate temperatures on structural, optical, wetting and electrical transport properties of CdS thin films.

In this work an effort has been made to investigate the photodetector of polycrystalline CdS nanoparticle NPs deposited on PSi wafer by drop casting method. The structural parameters of the CdS films and p-PSi samples were prepared and characterized by using X-ray diffractometer (Rigaku RUZHR, CuK α radiation) and JEOL (JSM-5600) scanning electron microscope SEM, FOURIER TRANSFORM INFRARED SPECTROPHOTOMETER (FTIR) made by Shimadzu respectively. The fundamental optical property which has been investigated here is the reflection of light at various wavelengths using Shimadzu (UV-Vis) Pharma Spec-1700 spectrophotometer and PL studies were made by Shimadzu fluoro-spectrophotometer (SL174) Xe Lamp power supply under 400nm excitation for pour. The shape and size of CdS nanoparticles were examined using field emission scanning electron microscopy ([FE-SEM Image Library](#)) and

*Corresponding author e-mail: ahmed_naji_abd@yahoo.com

transmission electron microscopy (type CM10 pw6020, Philips-Germany).

2 Methods

Crystalline wafer of p-type Silicon with resistivity of (2-20) $\Omega\cdot\text{cm}$, 508 μm thickness and (100) orientation were used as starting substrates. The substrates were cut into rectangles with areas of (1.5 \times 1.5) cm. After chemical treatment, 0.1 μm thick Al layers were deposited by using an evaporation method on the backsides of the wafer. Electrochemical etching then performed in a mixture (1:1) HF(40%) - Ethanol(99.99) at room temperature by using a (Au) electrode as in figure 1. 15 mA/cm² Current density was applied for 15 min etching time and the etched area of sample was (0.785 cm²).

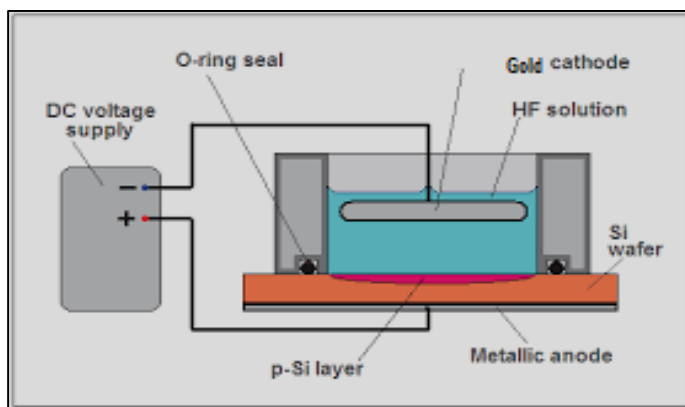


Fig. 1: Schematic diagram of the electrochemical etching set-up.

Cadmium sulfide CdS nanoparticles NPs were produced by laser ablation of CdS pressed pellet having diameter of 1cm² in methanol at room temperature. The CdS target was placed in the bottom of quartz vessel filled with 5ml of solution above the target. The colloidal solutions were synthesized by irradiating of CdS pellet with pulsed Nd:YAG laser operated at $\lambda=1064\text{nm}$ (type HUAFEI), 7ns pulse width and 10Hz repetition. The laser fluence used for ablation was fixed at 1.32 J/cm² and the ablation time was 5min as shown in figure 2a. Figure 2b shows a freshly CdS colloidal nanoparticles NPs prepared with 1.32 J/cm² laser fluence. The colloidal CdS NPs have different colors. The color of fresh CdS colloidal suspension have found to be depended on the laser fluence, for CdS NPs synthesised at low laser fluence 1.32 J/cm² was brown. where shorter wavelength, higher energy, electron transition correspond to smaller crystal size. CdS are a visually engaging way to demonstrate quantum effects in chemistry, since their transition energies can be explained as a "particle in a box," where a delocalized electron is the particle and the nanocrystal is the box.

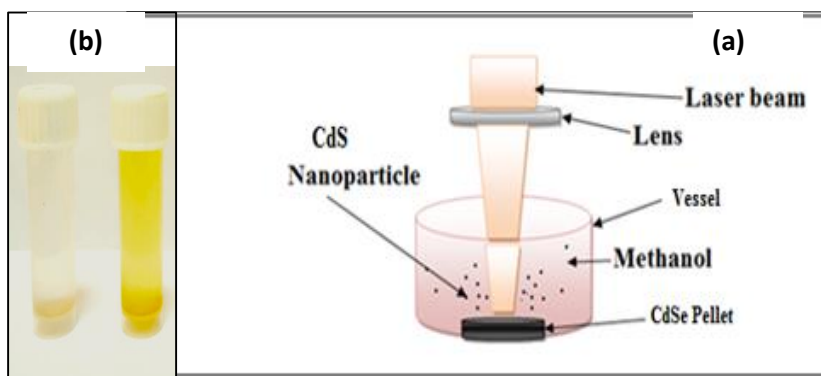


Fig. 2: a) Schematic diagram of laser ablation in liquid system and (b) CdS colloidal nanoparticles which are prepared with 1.32 J/cm² laser fluence.

Figure 3 shows that CdS colloidal nanoparticles which are prepared with 1.32 J/cm² laser fluence are deposited by drop casting technique on PSi layer. It has been taken from the solution by pipette and then drop on PSi/Si surface only 5 drops, then waiting for (5-6 hours) until dry under room temperature, then the film is ready.

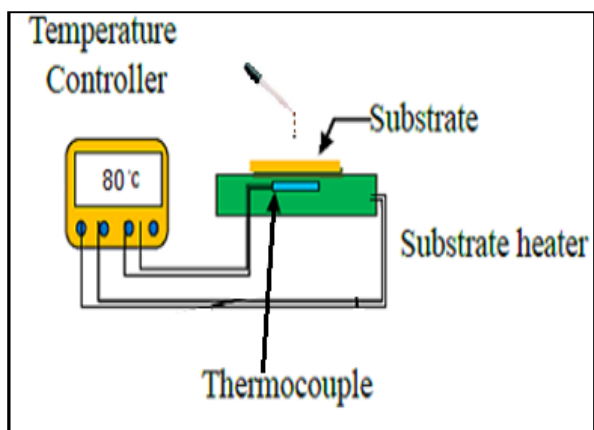


Fig. 3: Schematic diagram drop casting method experimental set up.

3 Results and Discussion

3.1 Morphology, Structure and Optical Studies Of Cds Nanoparticles NPS

The TEM images for CdS nanoparticles ablation in methanol shown in figure 4a .The micrographs confirm the formation of well-defined spherical nanoparticles also, shows that the CdS NP_s prepared with 1.32 J/cm² laser fluence have different size, it vary from 10 to 45 nm. These NP_s have quasi-spherical shapes. Figure 4b shows SEM images of CdS nanoparticles NPs prepared with 1.32 J/cm². SEM image confirmed that these NPs have different morphology, it can revealed that the morphology of CdS NPs is not uniform and consists of many small irregular nanoparticles with average size ranging from 35 to 60 nm.

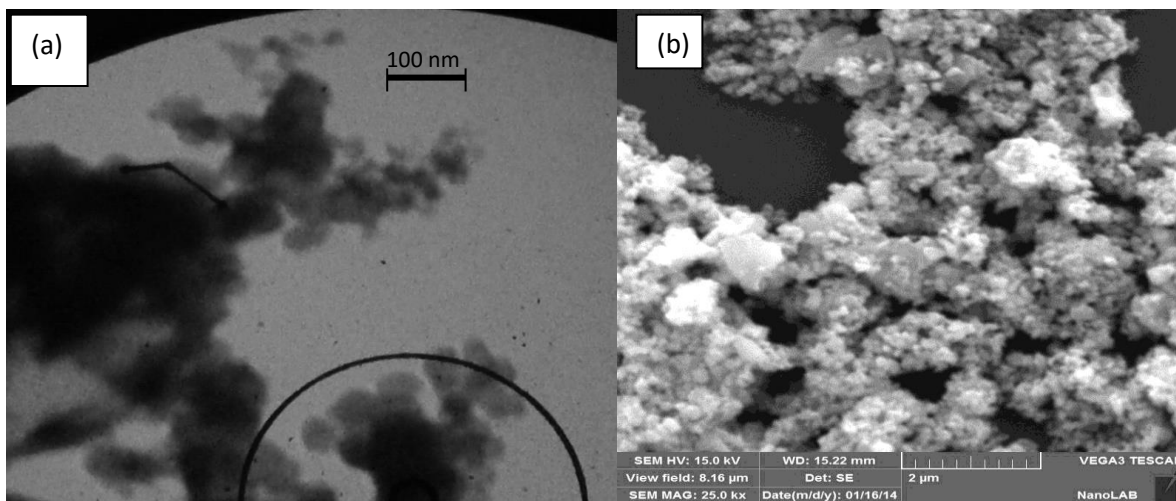


Fig. 4: a) TEM and b) SEM images of CdS colloidal nanoparticles dissolved in methanol and prepared with 1.32 J/cm² laser fluence.

Atomic force microscopic (AFM) allows us to get microscopic information on the surface structure and to plot topographies representing the surface relief. This technique offers digital images which allow quantitative measurements of surface features, such as root mean square roughness is (0.067 nm), RMS (0.0856) and the grain size (35 nm) as shown in figure (5).

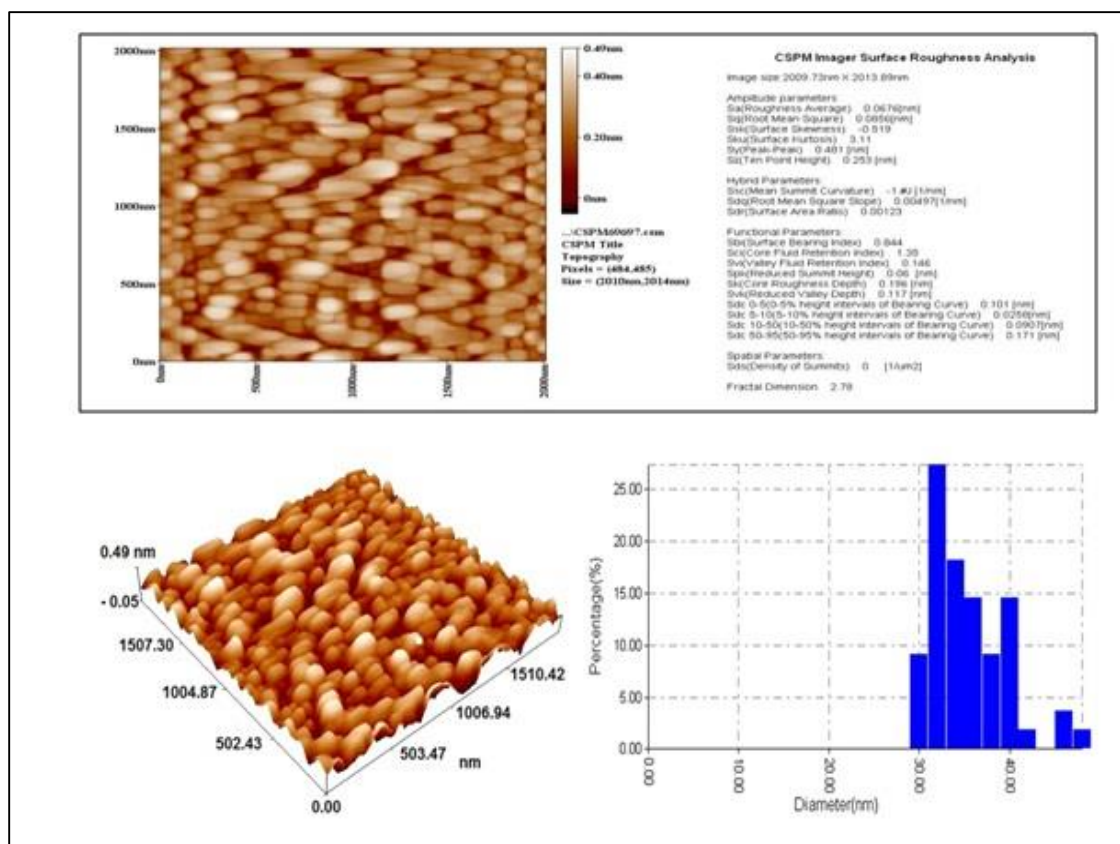


Fig. 5: 3D, 2D AFM images and Granularity accumulation distribution chart of CdS nanoparticles ablation in methanol with 1.32 J/cm^2 laser fluence.

The pattern shows hexagonal CdS structure, composing of the (100), (002), (101), (102), (110) and (103) peaks - corresponding to the JCPDS no. 41-1049 [5] ($a = b = 4.1409 \text{ \AA}$ and $c = 6.7198 \text{ \AA}$). Intensity of the (002) and (100) peaks of the product appears as the sharpest and strongest - implying that CdS crystals preferred to orient along the a and c axis respectively, and the product grew in the [100 and 002] directions [6,7].

Table 1. : Powder X-ray diffraction data of CdS.

laser fluence (J/cm^2)	2 theta (deg)	Plane (hkl)	β (deg)	d (\AA)	a (\AA)	D (nm)	$\sigma \times 10^{14}$ lines. m^{-2}	strain $\times 10^{-4}$ lines $^{-2} \text{m}^{-4}$
1.76	25.22	(100)	0.48	3.52	4.07	16.87	35.13	20.53
	26.87	(002)	0.43	3.31	8.97	18.67	28.66	18.55
	28.54	(101)	0.60	3.12	5.55	13.59	54.13	25.49

Figure 7 explain the transmission spectrum on CdS nanoparticles, from figure can notice that transmittance reach to 0.55 at 800 nm wavelength and this attribute to high transmittance of nanoparticles at these wavelength, then the transmission increased as s wavelength increased [16]. The crystallite size (D) was calculated using the Scherrer's formula, $D = 0.94 \lambda / \beta \cos\theta$, where λ (1.54056 \AA) is the X-ray wavelength, θ is the Bragg's angle and β is the full width at half maximum (FWHM) of the diffraction peak in radians. The calculated value of D is presented in Table 1. The average crystallite size was calculated by resolving (002) peak for hexagonal phase. It can be seen from the values of D that the as-grown CdS layer presents a nanocrystalline structure and an improvement of the grain size is observed in higher laser fluence, The micro-strain (ϵ) and dislocation density (δ) have been calculated using the following relations [31] and their values are presented in Table 2: micro-strain $\epsilon = \frac{\beta \cos\theta}{4}$ and dislocation density $\delta = \frac{1}{D^2}$ where w is the FWHM and D is the crystallite size. It is observed that the micro-strain and dislocation density increases by increasing laser fluence.

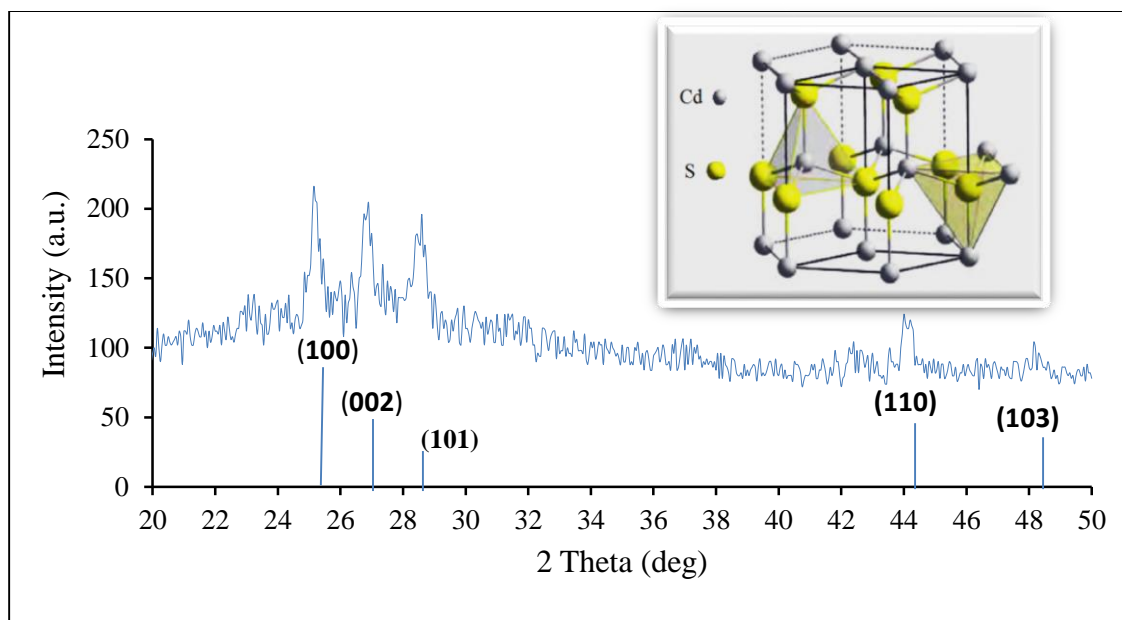


Fig. 6: XRD pattern of CdS nanoparticles films ablated in methanol with 1.32 J/cm² laser fluence.

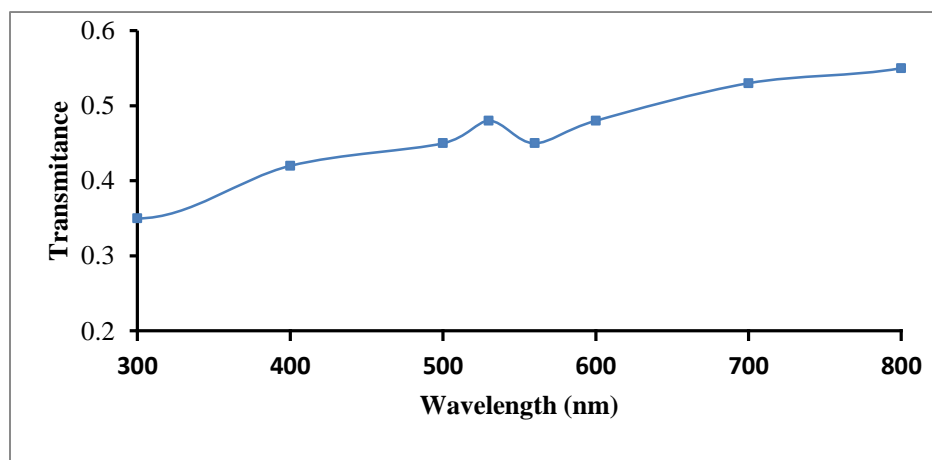


Fig. 7: Optical transmittance of CdS colloidal dissolved in methanol varies with 1.32 J/cm² laser fluence.

It can be clearly seen that the absorption and luminescence peaks of the CdS QDs were blue- shifted with decreasing laser fluence. The absorption spectra show an excitonic peak from 540 to 560 nm. Absorption spectra's with clear excitonic indicate mono dispersion of the CdS QDs. With decreasing QDs size. The observed blue-shift agrees with the optical bandgap (E_g) calculated from the Absorption peaks. From the transmission data, nearly at the fundamental absorption edge, the values of absorption coefficient α are calculated in the region of strong absorption using the following equation [17:

$$\alpha = \frac{1}{t} \ln \frac{1}{T} \dots \dots \dots (2)$$

Where t is the thickness and T transmission. The energy gaps E_g of CdS nanoparticles was estimated using Tauc relation [14] see fig 3:

$$\alpha h\nu = A(h\nu - E_g)^{\frac{1}{2}} \dots \dots \dots (3)$$

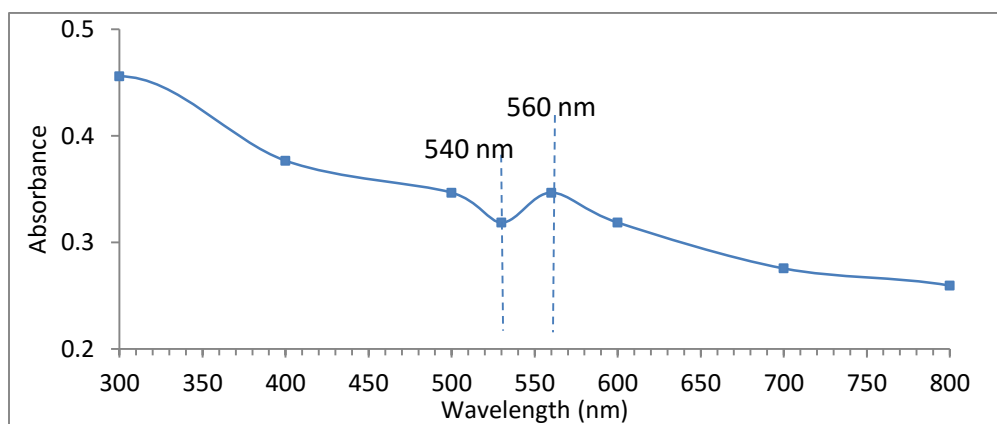


Fig. 8: Optical absorbance CdS colloidal dissolved in methanol with 1.32 J/cm^2 laser fluence

Where α is the absorption coefficient, E_g is the band gap energy, A is constant $h\nu$ is the photon energy. The band gap was determined from figure (9), which shows a plot of $(\alpha h\nu)^2$ versus $h\nu$ for CdS nanoparticles the intercept of the straight line with the $h\nu$ axis gives the band gap (E_g) 2.9 eV due to quantum confinement. The band gap energy is inversely proportional to the square of the particle radius.

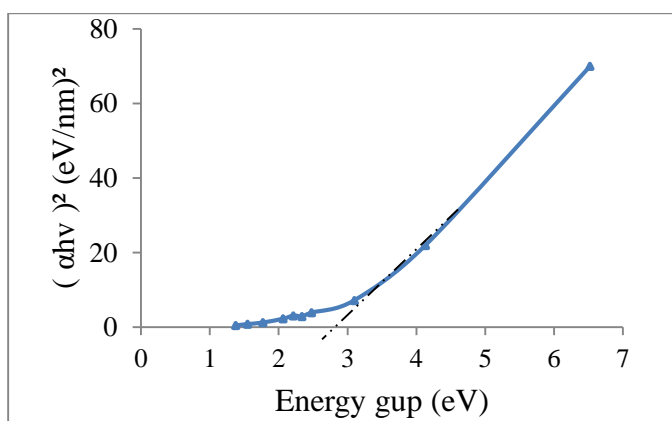


Fig. 9: Tauc's plots for CdS film .

3.2 Morphological and Structural Properties of porous silicon (PSi)

The microstructure of porous silicon (PSi) samples prepared with 15 mA/cm^2 current density and 15 min etching time was investigated using optical microscopy. These micrographs revealed that the PSi morphology can easily be recognized through the film homogeneity and color as shown in figure 11. The images exhibited high density of small pores distributed over the etched region. Also, the etched surfaces were rough and exhibited different colors; neither crack nor void are noticed on layer surface. This confirms the anodic dissolution of the silicon surface leading to porous structure formation and the visual observation of the silicon surface is considered as a very important feature that gave photoluminescence.

The surface morphology of the PSi/p-Si layer investigated by the AFM analyses is shown as a very smooth and homogeneous structure. The average roughness increases with the etching time. The film consists of a matrix of randomly distributed nanocrystalline silicon pillars which have the same direction as shown in figure 11. X-ray diffraction spectra show a distinct variation between the fresh silicon surface and PSi surfaces formed at different etching times. A strong peak of (PSi) at 5 min etching time shows a very sharp peak at $2\theta = 69.7^\circ$ oriented only along the (400) direction, which is observed, confirming the monocrystalline structure of the PSi layer which belongs to the (400) reflecting plane of Si of cubic structure (according to ICDD N 1997 and 2011 JCPDS).

The broadening in the diffracted peaks is due to the increasing thickness of pore walls, and upward shifts are due to relaxation of strain in the porous structure. XRD spectra show the porous silicon formation and that the structure is amorphous at 15 mA/cm^2 current density and 15 min etching time as shown in figure 12.

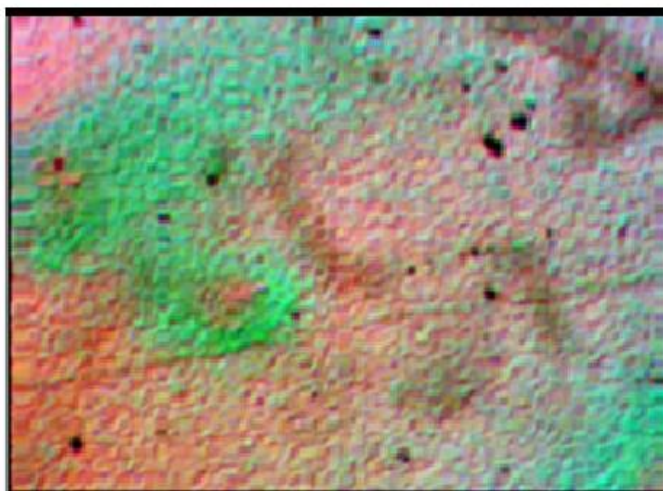


Fig. 10: Optical micrographs of p-PSi prepared with 15 mA/cm^2 etching current densities and 15min etching time, ($M=1000$)

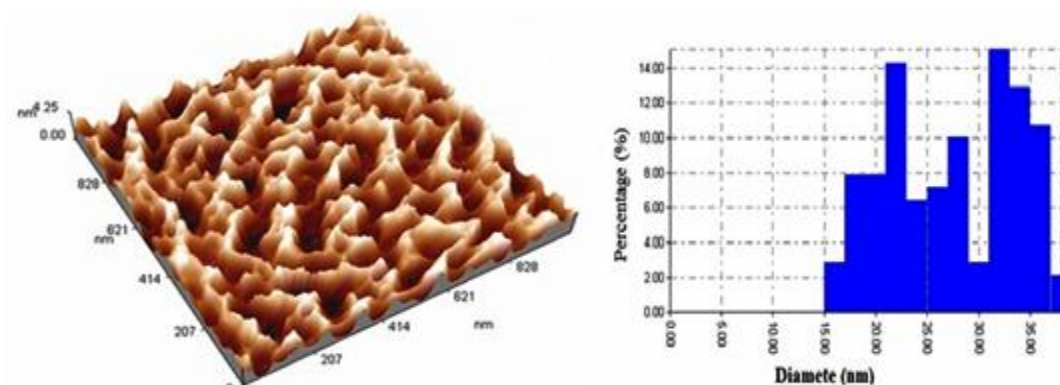


Fig. 11: 3D AFM images of p-PSi surface and Granularity accumulation distribution chart of CdS NPs synthesized at 15 mA.cm^{-2} and 15 min etching time.

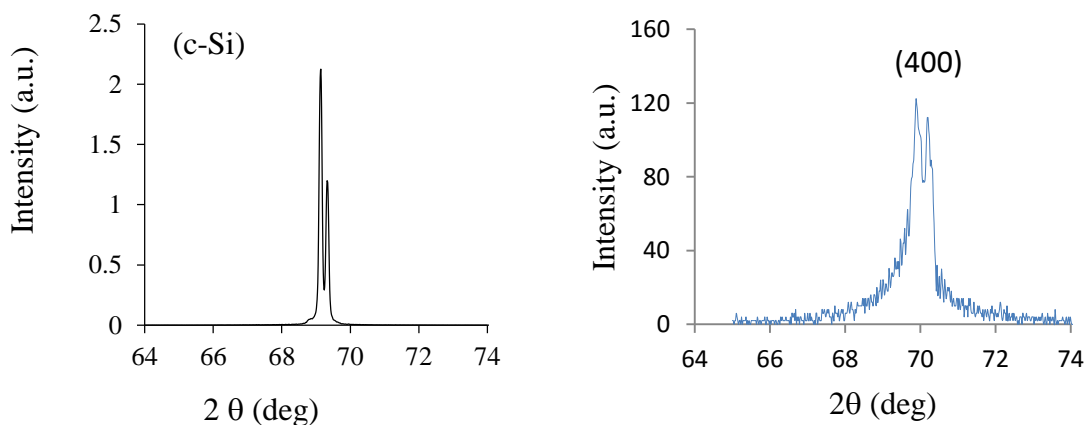


Fig. 12: XRD spectra of p-PSi samples anodized for c-Si and PSi/p-Si with 15 mA/cm^2 etching current density and 15 min etching time from left to right.

From FTIR data and Figures 13 for PSi /p-Si respectively, synthesized by 7 mA/cm^2 etching current density and 15 min etching time, it is clear that there are three distinct peaks with different intensities. The peak with intensity at 1080 cm^{-1} indicates the presence of Si-O-Si wagging, a small peak at 624 cm^{-1} can be associated with the Si-H Waggener mode. While a peak at 2854 cm^{-1} suggests the C-H stretching. A strong broad band is observed at about 1080 cm^{-1} due to Si-O-

Si asymmetry stretching vibrations mode in p-Si and n-Si type. The weak absorption bands centered at about 624cm^{-1} are attributed to the wagging modes of the SiH_x species. Absorption at 2854cm^{-1} and 2924cm^{-1} is due to the plane C-H angle deformation. It can easily replace a silicon atom, leading to the presence of carbon in the porous structure, since carbon is located in the same column of the periodic table as silicon [19]. Upon anodization in air, new chemical bonds appear on the surface as a wide transmission band due to different Si-H and Si-O chemical bond configurations in the IR spectra.

Also note that if a molecule is so symmetrical that the stretching of a bond does not produce any change in dipole moment, then no IR peak will be found in the spectrum [20].

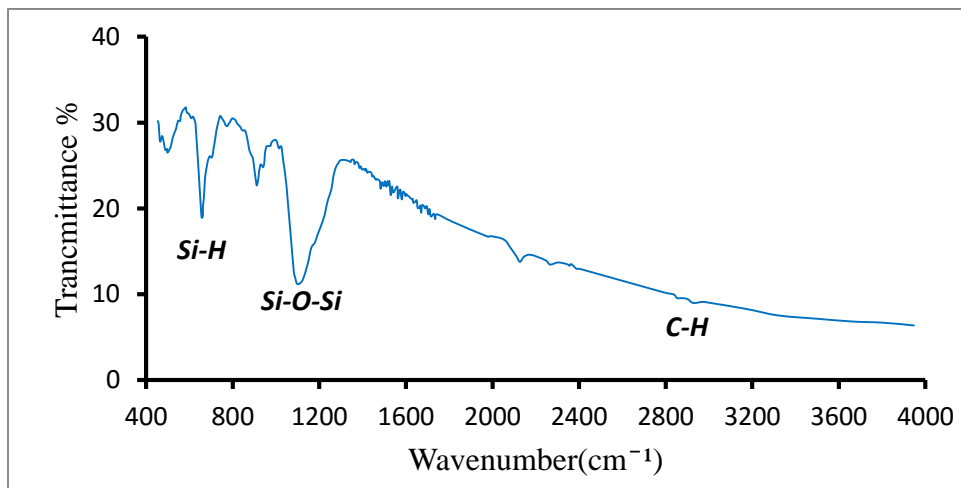


Fig.13: FTIR spectra of the PSi.

3.3 CdS/PSi/Si Hetrojunction Photodetector properties

Figure 15 shows that the CdS particle are deposited on the surface porous silicon and the other are diffused inside the pores. The bigger particles are agglomerated as a spherical or cubic shape with different grain size on the surface and the particles which gave size less than the pore size are diffused inside the pores .

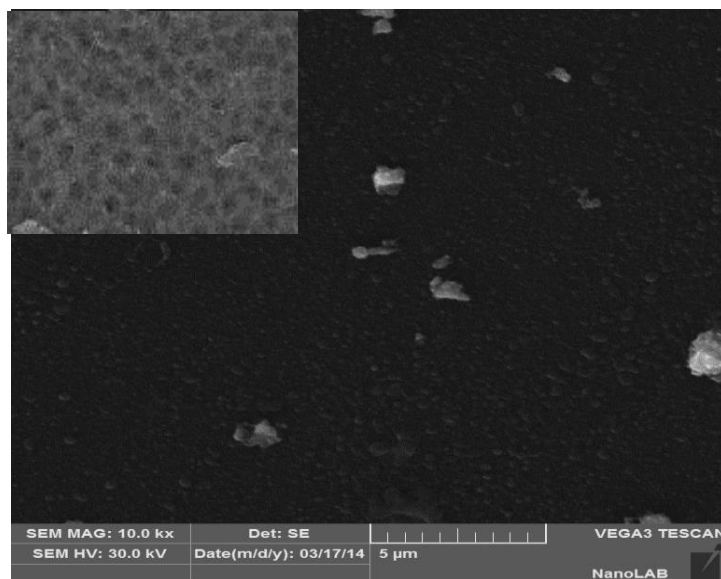


Fig. 14: SEM images of CdS film on porous silicon

Figure 15 shows the I-V dark characteristics in forward and reverse direction of Al/CdS/PSi/p-Si/Al Photodetector prepared with current density $15\text{mA}/\text{cm}^2$ and with constant etching time (15 min). The forward current of Photodetector is very small at voltage less than 2 V. This current is known as *recombination current* which occurs at low voltages only. It is generated when each electron excited from valence band to conductive band. The second region at high voltage represented

the diffusion or bending region which depending on series resistance. In this region; the bias voltage can deliver electrons with enough energy to penetrate the barrier between the two sides of the junction.

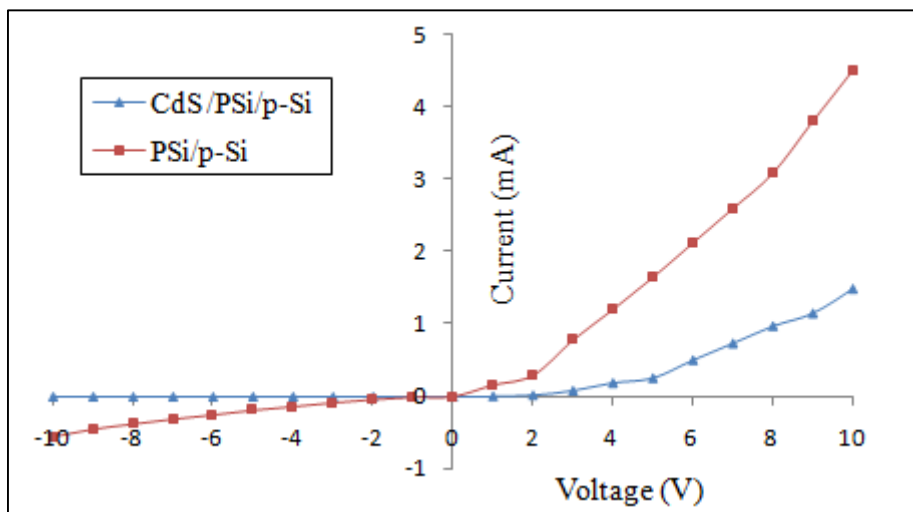


Fig. 15: I-V characteristic under forward reverse bias of the CdS/PSi/p-Si.

From figure 16 shows that the variation of $\ln(I_f)$ with bias voltage of CdS/PSi/p-n-Si heterojunction prepared with 15 min etching time and 7 mJ/cm^2 etching current density. The ideality factors of heterojunctions are estimated. Ideality factor was found to be around 1.44 for CdS/p-PSi heterojunction depending on etching current density, etching time and laser fluence. When the structure has a series resistance and interface states, ideality factor becomes higher than unity; most practical Schottky diodes show deviation from the ideal thermionic theory. The fact that such recombination currents are flowing not homogeneously in the structure, but always at local sites.

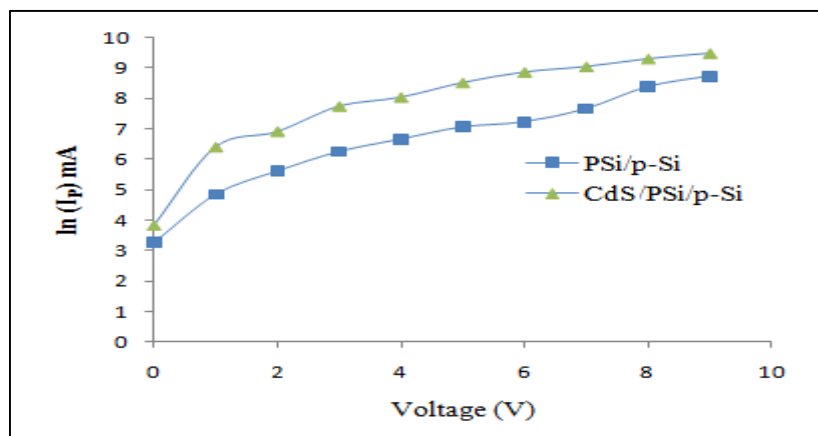


Fig. 16: Variation of $\ln(I_p)$ with bias voltage of CdS/p-PSi heterojunction.

Figure 17 shows that the reversed current-voltage characteristics of the device measured in dark and the photocurrent under a 41 W/m^2 tungsten lamp illumination. It can be seen that the reverse current value at a given voltage for CdS/PSi/p-Si heterojunction under illumination is higher than that in the dark and it can be seen from these figures that the current value at a given voltage for CdS/PSi/p-Si under illumination is higher than that in PSi/p-Si, this indicates that the light generated carrier –contributing photocurrent due to the production of electron –hole as a result of the light absorption. This behavior yields useful information on the electron-hole pairs, which are effectively generated in the junction by incident photons. The current of PSi/p-Si heterojunction is increased after deposition of CdSe nanoparticles film. This is ascribed to the increasing light absorption which leads to the increase in the creation of electron –hole pairs. Figure 18 shows that a linear relationship between C^{-2} and reverse bias voltage was obtained for the structure. This linear relationship represented the photodetector two heterojunctions between the (CdS/PSi) and (PSi/Si). The values of the built-in potential have been obtained and it has been found 0.5 volt depending on the etching time and current density. It represents the energy required by the electron to transfer from the CdS to PSi then from PSi to Si.

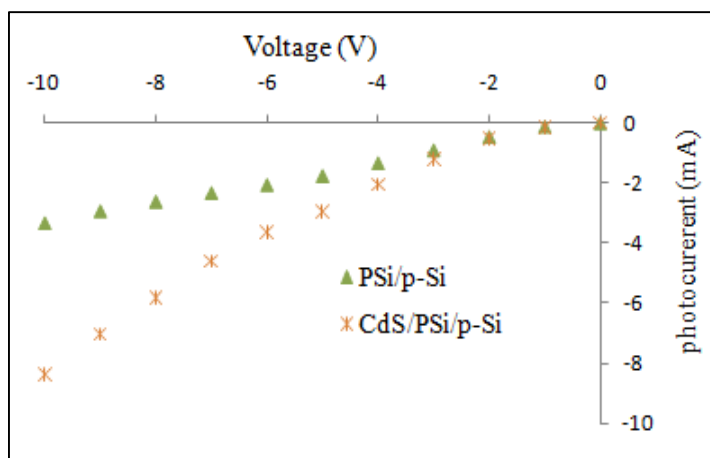


Fig. 17: illuminated (I-V) characteristic of CdS/PSi/p-Si and PSi/p-Si photodetectors .

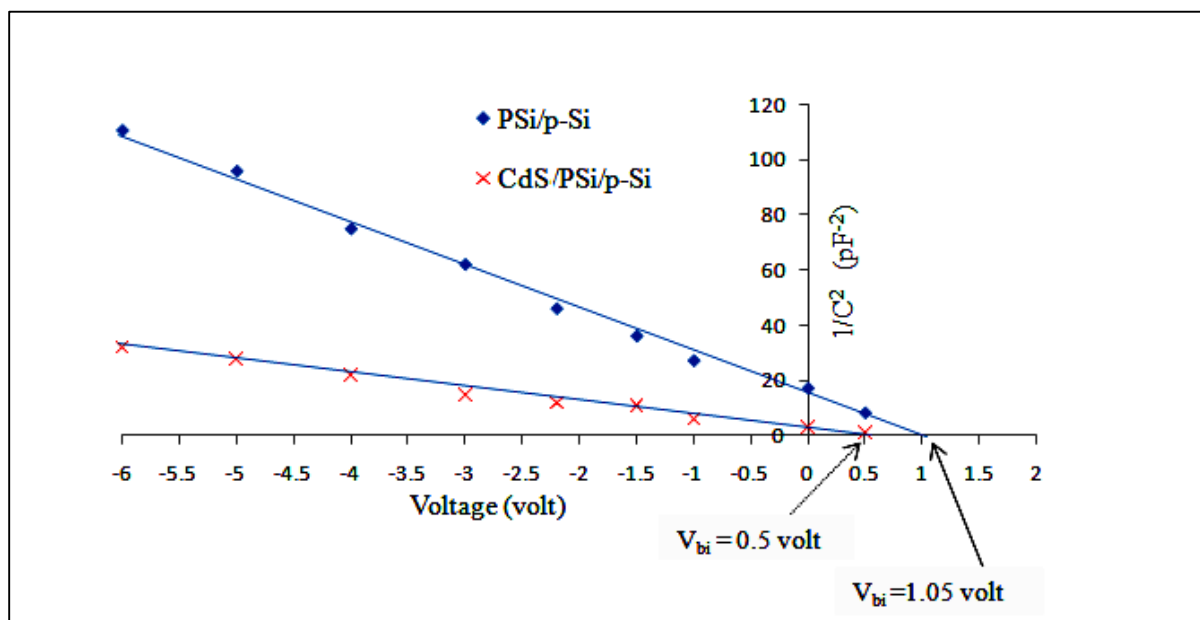


Fig. 18: $1/C^2$ versus reverse voltage of CdS/PSi/p-Si and PSi/p-Si Photodetectors.

Figure 19 displays the responsivity as a function of wavelength for CdS/PSi/p-Si Photodetector synthesized at 15 min etching time and 15 mA/cm^2 current density. It is clear from the figure the maximum responsivity is located at visible region and the other at the NIR region, the spectral responsivity curve of CdS/PSi/p-Si consists of two peaks of response; the first peak is located at 415 nm due to the absorption edge of CdS nanoparticles, while the second region is located at 770 nm due to absorption edge of silicon. Also, the figure shows that the specific detectivity as a function of wavelength for CdS/PSi/p-Si Photodetector and the detectivity is depend directly on responsivity. The maximum D^* found to be $6.8 \times 10^{12} \text{ W}^{-1} \cdot \text{cm} \cdot \text{Hz}^{1/2}$ at wavelength 770 nm for CdS/PSi/p-Si Photodetector.

Figure 20 shows that best photodetectors have higher life time ($320 \mu\text{sec}$) at (10 mA/cm^2) etching current density and 15 min etching time. It means that the probability of recombination will decrease. The lower life time ($28.5 \mu\text{s}$). Etching current density plays a significant role in controlling the device carrier life time (τ) and our result directly affected the estimated value of (τ) and related detector parameter. In this study it is found that measurements on multi-crystalline (Al/CdS/PSi/p-Si/Al) are not accuracy with this system possibly due to capacitive effects and/or back surface recombination effects.

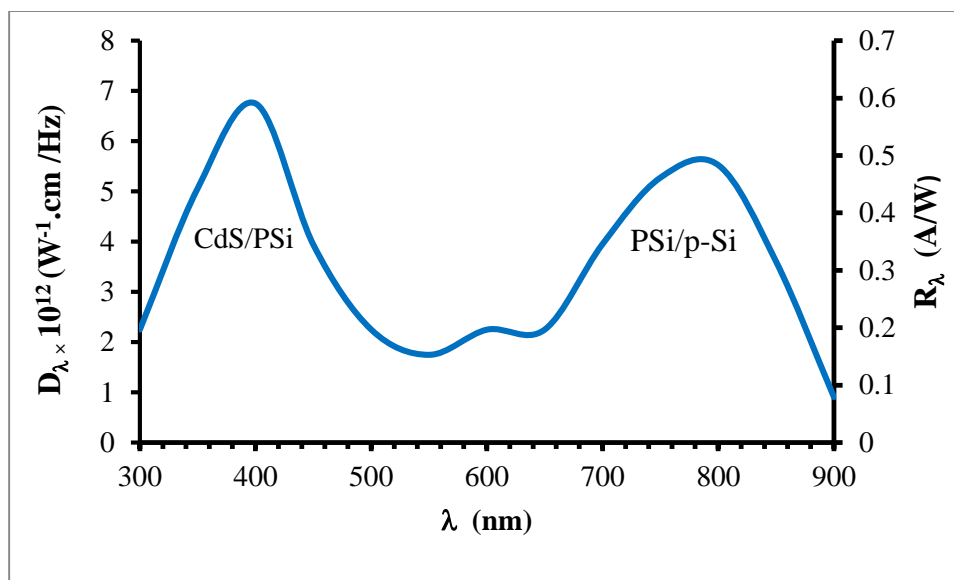


Fig. 19 : Spectral Responsivity and Spectral Detectivity plots for CdS/PSi/p-Si as a function of wavelength.

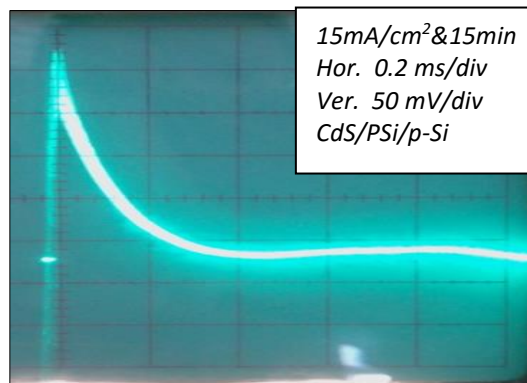


Fig. 20: Images for the Open-Circuit Voltage Decay Photograph with $15 J/cm^2$ etching current density and 15 min etching time.

4 Conclusions

The synthesised CdS NPs were in nanosized 25 nm prepared in methanol by laser ablation in liquids method and the optical properties revealed that the direct band gap of CdS NPs indicated to the effect of quantum size. X-ray diffraction (XRD) measurement disclosed that the CdS NPs are polycrystalline and have hexagonal crystal structure and no other phases were noticed, transmission electron microscopy (TEM) and Scanning electron microscopy (SEM) demonstrated that the CdS NPs prepared in toluene are bigger than those ablated in methanol due to high density of toluene.

Deposition of CdS NPs on porous silicon (PSi) gave suspensions photodetector characteristics enhanced the properties porous photodetectors. The spectral responsivity (R_λ) of Al/CdS/PSi/Si/Al photodetector was around 0.5 A/W at ≈ 780 nm wavelength due to the absorption edge of silicon and around 0.6 A/W at ≈ 415 nm wavelength due to the absorption edge of CdS NPs. The maximum value of the specific detectivity (D_λ) found to be $6.8 \times 10^{12} W^{-1}.cm.Hz^{-1}$ located at 770 nm wavelength for Al/CdS/PSi/Si/Al photodetector.

References

- [1]. Rao C.N.R., Kulkarni G.U., & Thomas P.J., "Nanocrystals: Synthesis, Properties and Applications" Springer, (2007) 9.
- [2]. Liz-Marzán L.M., & Kamat P.V., "Nanoscale Materials" Kluwer Academic Publisher, London, (2003) 5.
- [3]. Brus L. E. "Electron-electron and electron hole interactions in small semiconductor crystallites: The size dependence of the lowest excited electronic state" J. Chem. Phys. 80, 9 (1984) 4403.

- [4].Dzhafarov T.D., Ongul F., Yuksel S.A.," Effect of indium diffusion on characteristics of CdS films and nCdS/pSi heterojunctions", 84, 2, (2010) 310.
- [5] Powder Diffract. File, JCPDS Internat. Centre Diffract. Data, PA, U.S.A. (2001) 19073–3273.
- [6].Oladeji I.O., Chow L., Ferekides C.S., Viswanathan V., & Zhao Z., "Metal/CdTe/CdS/ Cd_{1-x}ZnxS/TCO/glass: a new CdTe thin film solar cell structure" Sol. Energy Mater. Sol. Cells,, 61, 2, (2000) 203.
- [7]. Brus L.E.," Quantum crystallites and nonlinear optics" Appl. Phys. A: Mater. Sci. Process. , 53(1991) 465.
- [8] Stokes AR, Wilson ACJ. Proc Phys Soc, 56 (1944) 174.
- [9].Murugan A. V., Kale B. B., Kulkarni A. V., Kunde L. B., & Saaminathan V. "Novel approach to control CdS morphology by simple microwave-solvothermal method" J. Mater. Sci.: Materials in Electronics, 16, 5 (2005) 295.
- [10].Jinxin Z., Gaoling Z., & Gaorong H.," Preparation of CdS nanoparticles by hydrothermal method in micro emulsion" Front. Chem. China. 2, 1 (2007) 98.
- [11].Gong W., Zheng Z., Zheng J., Hu X., & Gao W.," Water soluble CdS nanoparticles with controllable size prepared via femtosecond laser ablation" J. App. Phys. 102, 6 (2007) 064304.
- [12] Stewart M.P., Buriak J., Chemical and biological applications of porous silicon technology, Adv.Mater. 12 (2000) 859–869.
-